Doping Elemental 2D Semiconductor Te through Surface Se Substitutions

Guangyao Miao (苗光耀),[1,2] Nuoyu Su (苏诺雨),[1,3] Ze Yu (喻泽),[1] Bo Li (李博),[1] Xiaochun Huang (黄筱淳),[1] Weiliang Zhong (衷惟良),[1] Qinlin Guo (郭沁林),[1] Miao Liu (刘淼),[1] Weihua Wang (王炜华),[1,*] and Jiandong Guo (郭建东)[1,3,†]

[1]*Beijing National Laboratory for Condensed Matter Physics and Institute of Physics, Chinese Academy of Sciences, Beijing 100190, China*

[2]*Department of Physics & Center for the Science of Materials Berlin, Humboldt-Universität zu Berlin, Berlin 12489, Germany*

[3]*School of Physical Sciences, University of Chinese Academy of Sciences, Beijing 100049, China*

(Received 13 December 2023; accepted 24 October 2024; published 3 December 2024)

The development of two-dimensional (2D) semiconductors is limited by the lack of doping methods. We propose surface isovalent substitution as an efficient doping mechanism for 2D semiconductors by revealing the evolution of the structure and electronic properties of 2D Se/Te. Because of the different electronegativity of Se and Te, Se substitution for Te at the specific lattice sites introduces electric dipoles and leads to charge redistribution, which lowers the work function and tunes the Te films from *p*-type to *n*-type semiconductors. This differs from the gap enlargement of alloy films with random Se-Te substitutions. This doping method minimizes the change of lattice structure and surface roughness, which benefits structure stacking. Further increasing the Se content leads to the formation of two types of 2D semiconducting Se polymorphs.

DOI: 10.1103/PhysRevLett.133.236201

Semiconducting two-dimensional (2D) van der Waals materials such as transition metal chalcogenides and elemental atomic crystals have good structural stability and are characterized by the absence of dangling bonds. These materials are promising as next-generation electronic and optical devices [1–10]. Doping is a crucial technique for adjusting the band structure and reducing the difference in work function between the electrode and the 2D semiconductors, which is of great value in both fundamental research and device applications [11–15]. Applying traditional doping techniques on 2D semiconductors typically introduces significant charge or lattice disorder and the Fermi level pinning effect, degrading the performance of related devices [13,16–18]. Therefore, efficient doping methods without the Fermi level pinning effect and a clear understanding of the mechanism are urgently needed for the further development of 2D semiconductors. So far, doping of 2D semiconductors has been achieved by coating or intercalation of charge-transferring molecules or atoms [19–25], thickness engineering [26,27], surface functionalization [28–30], and atomic substitutions [31–34]. The introduction of isovalent substitutional dopants with same-group elements results in fewer disordering and has been extensively exploited [35–37]. However, the impact of surface isovalent substitutions on the electronic properties of the 2D semiconducting systems remains an open question.

We select the 2D Se/Te as a model system to study the impact of surface isovalent substitutions since Se and Te have significantly different electronegativity but could share the same helical crystal structure [38]. Trigonal tellurium has attracted significant research interest due to its excellent physical properties, including outstanding thermoelectricity [39–41], high carrier mobility [42–44], midinfrared polarized photoresponse [45–47], chiral edge states [48], spin-polarized band structure, possessing Weyl fermions [49–52], and novel electronic-magnetic coupling effect [53,54]. While pure Te is a *p*-type semiconductor [50,55,56]. Electron doping in bulk Te crystals and thick Te films has been achieved through potassium deposition or the dielectric doping technique of atomic layer deposition [25,49,52]. When the thickness of Te approaches the 2D limit, tellurium exhibits multiple phases [57,58], thickness-dependent band gap (0.33–1.0 eV) [42,59,60], and quasi-periodic edge defect states [61], making it a promising candidate in future energy and information devices. Nevertheless, an efficient doping method without compromising the lattice structure of ultrathin Te films is still lacking.

Here, we use molecular beam epitaxy (MBE), scanning tunneling microscopy, and spectroscopy (STM/STS), x-ray photoelectron spectroscopy (XPS), and density functional theory (DFT) calculations to study the doping effect of surface Se-Te substitutions (Se_{Te}). The substitutions introduce efficient electron doping and tune the ultrathin Te

*Contact author: weihuawang@iphy.ac.cn

†Contact author: jdguo@iphy.ac.cn

 © 2024 American Physical Society

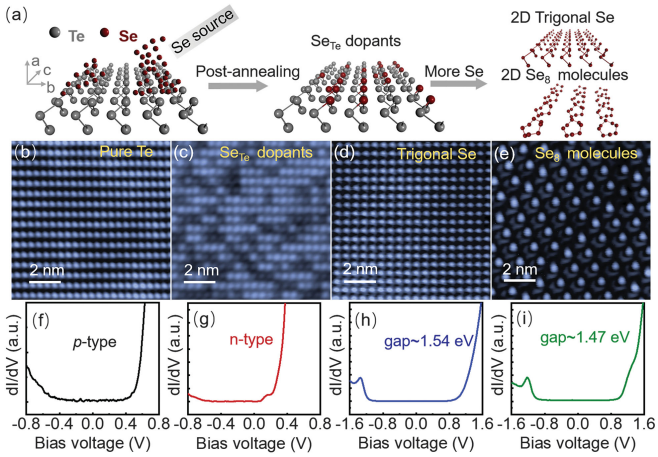

FIG. 1. Fabrication of Se/Te 2D structures. (a) Sketch of the evolution of the Se/Te 2D structures. (b)–(e) STM images of the pure Te film, Te film with surface Se_{Te} dopants, trigonal Se film, and Se_8 molecular crystal. Parameters: (b),(c), and (e) $V_b = -2$ V, $I_t = 100$ pA; (d) $V_b = -2$ V, $I_t = 50$ pA. (f)–(g) The differential conductance (dI/dV) spectra acquired on pure Te film (thickness ~4.6 nm), Te film with surface Se_{Te} dopants (thickness ~4.6 nm), trigonal Se film, and Se_8 molecular crystal.

films from p type to n type semiconductors without breaking the lattice structure. The doping mechanism is further revealed as the surface Se_{Te} substitutions form the surface dipole and accumulate the electrons on the surface, lowering the system's work function.

Se atoms are introduced to Te films by thermal evaporation and post-annealing in ultrahigh vacuum conditions [Fig. 1(a)]. Ultrathin trigonal Te films [Fig. 1(b) for atom-resolved STM image] are grown on graphene/SiC(0001) substrate following the reported methods [59,61]. Upon Se deposition with Te films held at room temperature and postannealing at ~60 °C, Se atoms substitute for surface Te atoms and form Se_{Te} substitutional dopants. By optimizing the Se dosage and postannealing conditions, we can get Te films with homogenously surface Se_{Te} dopants distribution at a few tens nm scale (See Fig. S1 for details) [62]. As shown in Fig. 1(c), the bright and dim atoms are distributed on the surface while the film maintains the lattice structure of Te. The Te films, both before and after adding surface Se_{Te} dopants, exhibit atomically flat Te terraces (Fig. S2) [62]. Benefiting from the flat surface, two different 2D Se crystalline structures, including trigonal Se and Se_8 molecular crystal, are further obtained [Figs. 1(d) and 1(e)]. The evolution of electronic structure is revealed by our STS measurements [Figs. 1(f)–1(i)] (See Fig. S3 for the details of determining band edges and carrier types [62], following the reported method [69]). The conduction band minimum (CBM) of surface Se-doped Te films can be tuned to ~38 meV above the Fermi level (345 meV for pure Te), showing the efficient doping effect. The fabricated 2D trigonal Se and Se_8 molecular crystals are both n-type semiconductors and feature larger band gaps.

Figures 2(a)–2(c) compare the atom-resolved STM images of Se-doped Te films with increased Se dosage after postannealing. They are different from the homogenous atom arrangement on pure Te film, showing bright (larger) and dim (smaller) atoms simultaneously. Though the detailed height analysis of the STM image acquired on

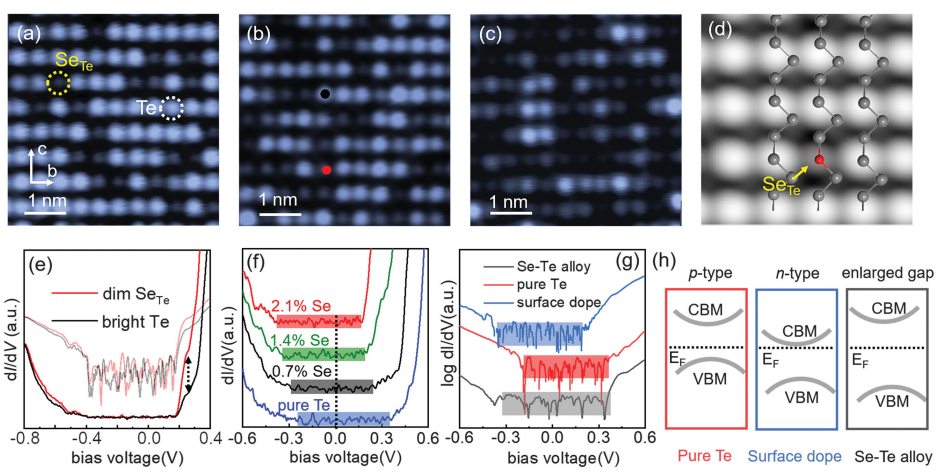

FIG. 2. STM and STS characterizations of Te films with surface Se_{Te} dopants. (a)–(c) Atom-resolved STM images of Te films with increased Se_{Te} concentration. Parameters: (a)–(c) $V_b = -1$ V, $I_t = 100$ pA. (d) The DFT simulated STM image of Se_{Te} dopant at $V_b = -1$ V with a structural model superposed. The red and grey balls represent Se and Te atoms, respectively. (e) Site-dependent dI/dV spectra measured on bright atoms and dim atoms, indicated by black and red dots in (b). The translucent curves show their logarithmic spectra. (f) dI/dV spectra measured on the pure and doped Te films with different Se concentrations and the same thickness. The curves are vertically shifted for clarity. The energy gaps are highlighted in different colors. All spectra are obtained on Te films with a thickness of 4.6 nm (~12 layers) to exclude thickness dependency and substrate doping. (g) The logarithmic dI/dV spectra of pure Te, Se-Te alloy, and surface Se-doped Te films (4.2 nm, ~11 layers). (h) The sketch of the electronic modulation of surface Se_{Te} dopants and Se-Te alloy.

the surface Se-doped Te films show some continuous distribution in the heights (due to the initial height fluctuation of pure Te film), the height statistics can still be well fitted in a binary peaks curve (see Figs. S4 and S5) [62]. Since the portion of dim atoms increases with Se dosage, they are assigned to Se_{Te} dopants. Our DFT simulated STM image of trigonal Te film with Se_{Te} further confirms this [Fig. 2(d)]. The dopants show relative homogenous distribution at the few tens nanometers scale but a clustering feature at the few nanometers scale. The further calculational results of the negative logarithm pair correlation function ($-\ln[C_{(r)}]$), which is proportional to the mean force potential [70–73], indicate that the paired Se_{Te} dopants show attractive interactions below 1 nm and maximum repulsive interaction at ~3 nm (Fig. S6) [62].

Figure 2(e) shows the typical differential conductance (dI/dV) spectra measured on the Te atom and Se_{Te} dopant on the same sample. Compared to the Te site, the Se_{Te} dopant exhibits a similar local density of states (LDOS) near the valence band maximum (VBM) and CBM energy but enhanced LDOS near the CBM. No in-gap state is observed on the Se_{Te} site, suggesting the free of Fermi level pinning effect, similar to the O_{Se} and O_S substitutional dopants in $MoSe_2$ and WS_2 [74]. The Se_{Te} dopants give rise to a dopant state near CBM, which has been reproduced by our DFT calculations (Fig. S7) [62]. As shown in Fig. 2(f), It is evident that by increasing Se_{Te} concentration, the p-type Te is modulated towards n-type with an enhanced dopant band. The Se_{Te} dopants also reduce the band gap from 0.63 eV of pure Te to 0.54 eV of Te with 2.1% Se content because of the overlap between the dopant band and the conduction band. The movement of the band structure versus the increased concentration of Se_{Te} dopants shows a logarithmic relation (Fig. S8) [62], which follows a Boltzmann distribution in a nondegenerate doping of semiconductors.

Through the surface method for introducing Se_{Te} substitutional dopants, only a small number of Se atoms replace the surface Te atoms. The angle-dependent XPS measurements show an increased area ratio of Se-$3d_{5/2}$/Te-$3d_{5/2}$ peaks with the increasing tilting angle of the sample, manifesting that the Se atoms mainly exist on the surface (see Fig. S9 in [62]). The surface Se_{Te} substitution at a specific lattice site is distinct from the Se-Te alloy regime. The Se-Te alloy film (see Fig. S10 for the STM images) [62] with the same thickness exhibits an enlarged band gap of 0.72 eV, much larger than pure and surface-doped Te films [Figs. 2(g) and 2(h)]. It is reasonable since pure trigonal Se has a larger band gap than pure Te. Furthermore, we find that the dopant band can be detected even near the doped region with almost no Se_{Te} dopants (Fig. S11) [62], suggesting that the doping effect of the Se_{Te} dopants is delocalized and free from the Fermi-level pinning effect. This is consistent with the distance-related interactions between the dopants analyzed through the pair correlation function discussed before.

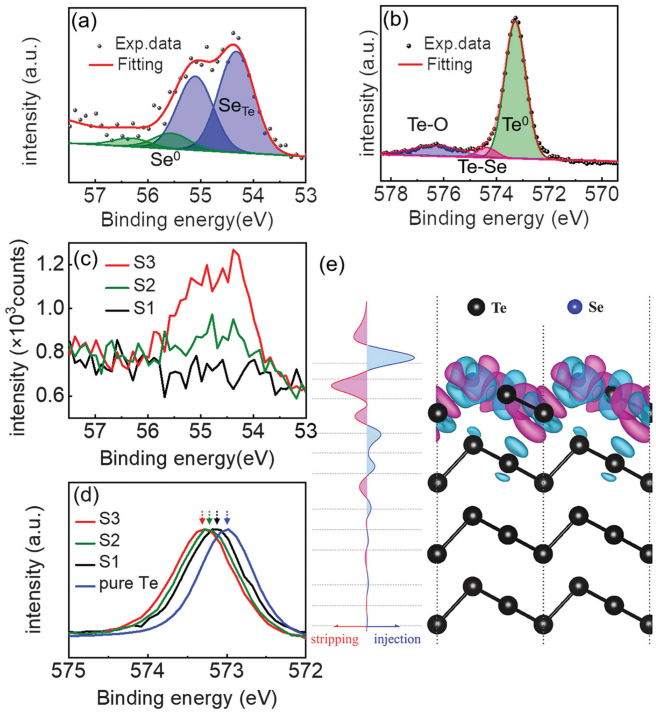

FIG. 3. XPS characterization and DFT calculation results. (a), (b) XPS Survey near the $3d_{5/2}$ and $3d_{3/2}$ peaks of Se (a) and Te (b) in the heavily surface Se doped sample. (c) Comparison of XPS results of three samples with different Se dosages. (d) Evolution of the Te-$3d_{5/2}$ peak with increased Se dosage. (e) DFT calculated charge redistribution at the surface of the Te film when Se_{Te} substitutional dopants are introduced. The left panel shows the electron stripping and injection situation along the film's normal direction.

To characterize the doping effect of the surface isovalent Se_{Te} dopants at the macroscale, we carried out an XPS survey on pure Te films and Te films with increased surface Se concentration. As shown in Fig. 3(a), the binding energies (BE) of Se $3d_{3/2}$ and $3d_{5/2}$ in a sample with high surface Se_{Te} concentration (S3) are shifted to 55.1 and 54.3 eV, ~1.3 eV lower than those in elemental Se (56.4 and 55.6 eV, respectively), indicating the negative valence state of Se atoms in Se_{Te} dopants. By fitting the Te $3d_{5/2}$ spectrum of the heavily doped sample in Fig. 3(b), three components are resolved: the weak feature at 576.4 eV (blue area) is assigned to oxidized Te^{2+}; the component at 574.4 eV, which is ~1.4 eV higher than that in pure Te, is assigned to those Te atoms bonding to Se atoms; the main peak at 573.3 eV is assigned to Te^0 atoms. Compared to pure Te, the BE of Te^0 atoms in the S3 sample is 0.3 eV higher, which is attributed to a decreased work function caused by the electron doping effect of surface Se_{Te} dopants. The Se $3d$ and Te $3d$ spectra in doped Te films with different Se dosages are compared in Figs. 3(c) and 3(d), respectively. With increased Se dosage, the Se $3d$ signal gets stronger, and the main peak shifts gradually from 573.0 eV in pure Te to 573.3 eV in heavily surface

Se-doped Te, which is consistent with the STS measurements [Fig. 2(f)]. The air sensitivity of the surface Se_{Te} substitution doping method is further explored by STM and XPS. The surface Se_{Te} doping did not lower the stability against air exposure of Te films (see Fig. S12) [62], showing its advantage over some charge transfer methods. In another aspect, the introduction of Se_{Te} substitutions does not lower the thermal stability of the films due to the stronger bonding of Se-Te than Te-Te [75].

To figure out the physical origin of the electron doping effect caused by the surface isovalent Se_{Te} dopant in Te films, we performed first-principles calculations to investigate the change in charge density before and after substituting Se for Te (see Supplemental Material [62] for details). The Se_{Te} substitution leads to charge density redistribution, introducing ripples in differential charge density (DCD) penetrating from the Se towards the inner layers of the film, at least two layers deep [Fig. 3(e)]. Electron accumulation occurs at the Se atoms, causing electron depletion at the Te atoms directly bonding to the Se atoms, which is consistent with the 1.3 eV BE shift seen in XPS experiments. Electrons also accumulate in the undoped second trilayer to balance the positive charge at the Te atoms bonding to Se. The Se-Te surface electron dipole induces a charge accumulation that reduces the films' work function. This strategy could also be applied to tune the surface work function of thicker films, which is helpful for lowering the contact resistance that mainly occurs at the interface of semiconductors and electrodes. Furthermore, this effect can be extended to various elemental 2D crystals with surface isovalent dopants. We demonstrate DFT calculations for a few layers of trigonal tellurium with surface S_{Te} substitutions and a few layers of arsenic in a black phosphoruslike structure with surface P_{As} substitutions. Both systems are stabilized under DFT relaxation, generating perpendicular electric dipoles and introducing charge redistribution similar to that in Se/Te (see Fig. S13) [62]. These results demonstrate the applicability of this doping mechanism to other elemental 2D semiconductors beyond the Se/Te case.

Increasing the Se dosage beyond the surface substitution regime cannot make the extra Se act as dopants further but form 2D Se structures, giving the upper limit of the surface doping method. Two types of crystalline Se films are observed: trigonal Se and Se_8 molecular crystals. The trigonal Se film has a similar structure to trigonal Te but with different lattice parameters [Fig. 4(a)]. The large-scale and zoomed-in STM images of trigonal Se show in-plane lattice constants $b = 0.45$ nm and $c = 0.55$ nm and a nominal height of 0.41 nm [Figs. 4(b) and 4(c)]. A tentative structural model of the molecular Se_8 film, calculated by the material database Atomly [76], is shown in Fig. 4(d). The Se_8 molecular film has a nominal height of 0.45 nm, an in-plane unit cell of $a = 0.81$, $c = 1.05$ nm (111°), which is close to the calculated structure ($a_0 = 0.89$, $c_0 = 1.12$ nm, and an angle of 105° between them) (see Figs. S14 and S15 for details) [62].

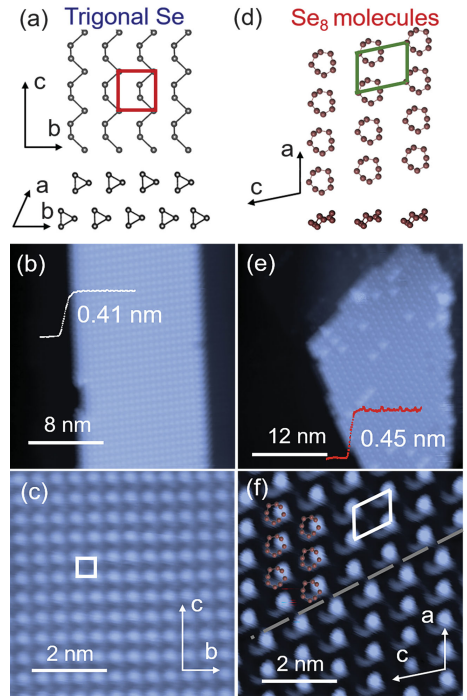

FIG. 4. 2D elemental selenium structures. (a) Crystal structure of trigonal Se. The upper panel and lower panel show the top view and side view, respectively. (b) and (c) Large-scale and atom-resolved STM images acquired on the ultrathin trigonal Se films. Parameters: (b) and (c) $V_b = -2$ V, $I_t = 50$ pA. (d) Calculated crystal structure of monolayer Se_8. The upper and lower panel shows the top view and side view, respectively. (e) and (f) Large-scale and atom-resolved STM images of monolayer Se_8 films. The Se_8 crystal structure is superposed on (f). Parameters: (e) $V_b = -2$ V, $I_t = 50$ pA, (f) $V_b = 1.5$ V, $I_t = 200$ pA.

In summary, we report the controllable doping on the ultrathin tellurium films by introducing surface Se_{Te} substitutions. The doping method has low processing temperature, efficient doping capacity, and some degree of air and thermal stability, compatible with the mainstream device preparation technology. The generalizability of this method is confirmed by the analogical calculations in S_{Te} and P_{As} systems. We propose that the electric dipole introduced by specific-lattice-sited isovalent substitutions could efficiently tune the work function of vast elemental 2D semiconducting materials, which paves the way for further development of elemental 2D semiconductors.

Acknowledgments—This work was supported by the Strategic Priority Research Program of the Chinese Academy of Sciences (Grant No. XDB33000000), and the National Natural Science Foundation of China (Grants No. 11974399, No. 12374198, No. 11974402).

G. M. acknowledges the support from the IOP-Humboldt postdoc fellowship in physics of the Institute of Physics, Chinese Academy of Sciences, and Integrative Research Institute for the Sciences of Humboldt-Universität zu Berlin.

[1] K. S. Novoselov, A. Mishchenko, A. Carvalho, and A. H. Castro Neto, Science **353**, aac9439 (2016).
[2] A. J. Mannix, B. Kiraly, M. C. Hersam, and N. P. Guisinger, Nat. Rev. Chem. **1**, 0014 (2017).
[3] M. Long, P. Wang, H. Fang, and W. Hu, Adv. Funct. Mater. **29**, 1803807 (2019).
[4] M. Macha, S. Marion, V. V. R. Nandigana, and A. Radenovic, Nat. Rev. Mater. **4**, 588 (2019).
[5] N. R. Glavin, R. Rao, V. Varshney, E. Bianco, A. Apte, A. Roy, E. Ringe, and P. M. Ajayan, Adv. Mater. **32**, 1904302 (2020).
[6] J. Fang, Z. Zhou, M. Xiao, Z. Lou, Z. Wei, and G. Shen, InfoMat **2**, 291 (2020).
[7] X. Zou, Y. Xu, and W. Duan, Innovation **2**, 100115 (2021).
[8] Y. Kang, H. Zhang, L. Chen, J. Dong, B. Yao, X. Yuan, D. Qin, A. V. Yaremenko, C. Liu, C. Feng, X. Ji, and W. Tao, Innovation **3**, 100327 (2022).
[9] S. Zeng, C. Liu, and P. Zhou, Nat. Rev. Electr. Eng. **1**, 335 (2024).
[10] K. S. Kim, J. Kwon, H. Ryu, C. Kim, H. Kim, E.-K. Lee, D. Lee, S. Seo, N. M. Han, J. M. Suh *et al.*, Nat. Nanotechnol. **19**, 895 (2024).
[11] S. Lee, A. Tang, S. Aloni, and H. S. Philip, Wong, Nano Lett. **16**, 276 (2016).
[12] D. Qi, Q. Wang, C. Han, J. Jiang, Y. Zheng, W. Chen, W. Zhang, and A. T. S. Wee, 2D Mater. **4**, 045016 (2017).
[13] Y. Liu, J. Guo, E. Zhu, L. Liao, S.-J. Lee, M. Ding, I. Shakir, V. Gambin, Y. Huang, and X. Duan, Nature (London) **557**, 696 (2018).
[14] P. Chen, T. L. Atallah, Z. Lin, P. Wang, S.-J. Lee, J. Xu, Z. Huang, X. Duan, Y. Ping, Y. Huang *et al.*, Nature (London) **599**, 404 (2021).
[15] D. Lee, J. J. Lee, Y. S. Kim, Y. H. Kim, J. C. Kim, W. Huh, J. Lee, S. Park, H. Y. Jeong, Y. D. Kim *et al.*, Nat. Electron. **4**, 664 (2021).
[16] C. Gong, L. Colombo, R. M. Wallace, and K. Cho, Nano Lett. **14**, 1714 (2014).
[17] N. Kaushik, A. Nipane, F. Basheer, S. Dubey, S. Grover, M. M. Deshmukh, and S. Lodha, Appl. Phys. Lett. **105**, 113505 (2014).
[18] X. Liu, M. S. Choi, E. Hwang, W. J. Yoo, and J. Sun, Adv. Mater. **34**, 2108425 (2022).
[19] W. Chen, S. Chen, D. C. Qi, X. Y. Gao, and A. T. S. Wee, J. Am. Chem. Soc. **129**, 10418 (2007).
[20] H. Lin, J. D. Cojal González, N. Severin, I. M. Sokolov, and J. P. Rabe, ACS Nano **14**, 11594 (2020).
[21] Y. He, F. Xia, Z. Shao, J. Zhao, and J. Jie, J. Phys. Chem. Lett. **6**, 4701 (2015).
[22] J. Guan, J. Liu, B. Liu, X. Huang, Q. Zhu, X. Zhu, J. Sun, S. Meng, W. Wang, and J. Guo, Phys. Rev. B **95**, 205405 (2017).
[23] Y. Gong, H. Yuan, C.-L. Wu, P. Tang, S.-Z. Yang, A. Yang, G. Li, B. Liu, J. van de Groep, M. L. Brongersma *et al.*, Nat. Nanotechnol. **13**, 294 (2018).
[24] L. Yang, K. Majumdar, H. Liu, Y. Du, H. Wu, M. Hatzistergos, P. Y. Hung, R. Tieckelmann, W. Tsai, C. Hobbs *et al.*, Nano Lett. **14**, 6275 (2014).
[25] C. Niu, G. Qiu, Y. Wang, M. Si, W. Wu, and P. D. Ye, Nano Lett. **21**, 7527 (2021).
[26] Z. Wang, H. Xia, P. Wang, X. Zhou, C. Liu, Q. Zhang, F. Wang, M. Huang, S. Chen, P. Wu *et al.*, Adv. Mater. **33**, 2104942 (2021).
[27] C. Zhou, Y. Zhao, S. Raju, Y. Wang, Z. Lin, M. Chan, and Y. Chai, Adv. Funct. Mater. **26**, 4223 (2016).
[28] S. Lei, X. Wang, B. Li, J. Kang, Y. He, A. George, L. Ge, Y. Gong, P. Dong, Z. Jin *et al.*, Nat. Nanotechnol. **11**, 465 (2016).
[29] A.-Y. Lu, H. Zhu, J. Xiao, C.-P. Chuu, Y. Han, M.-H. Chiu, C.-C. Cheng, C.-W. Yang, K.-H. Wei, Y. Yang *et al.*, Nat. Nanotechnol. **12**, 744 (2017).
[30] A. Sahu, B. Russ, M. Liu, F. Yang, E. W. Zaia, M. P. Gordon, J. D. Forster, Y.-Q. Zhang, M. C. Scott, K. A. Persson *et al.*, Nat. Commun. **11**, 2069 (2020).
[31] J. Suh, T.-E. Park, D.-Y. Lin, D. Fu, J. Park, H. J. Jung, Y. Chen, C. Ko, C. Jang, Y. Sun *et al.*, Nano Lett. **14**, 6976 (2014).
[32] J. Tang, Z. Wei, Q. Wang, Y. Wang, B. Han, X. Li, B. Huang, M. Liao, J. Liu, N. Li *et al.*, Small **16**, 2004276 (2020).
[33] J. Pető, T. Ollár, P. Vancsó, Z. I. Popov, G. Z. Magda, G. Dobrik, C. Hwang, P. B. Sorokin, and L. Tapasztó, Nat. Chem. **10**, 1246 (2018).
[34] J. Zhou, J. Lin, X. Huang, Y. Zhou, Y. Chen, J. Xia, H. Wang, Y. Xie, H. Yu, J. Lei *et al.*, Nature (London) **556**, 355 (2018).
[35] Q. Liang, J. Gou, Arramel, Q. Zhang, W. Zhang, and A. T. S. Wee, Nano Res. **13**, 3439 (2020).
[36] C.-Z. Chang, J. Zhang, X. Feng, J. Shen, Z. Zhang, M. Guo, K. Li, Y. Ou, P. Wei, L.-L. Wang *et al.*, Science **340**, 167 (2013).
[37] F. Li, H. Ding, C. Tang, J. Peng, Q. Zhang, W. Zhang, G. Zhou, D. Zhang, C.-L. Song, K. He *et al.*, Phys. Rev. B **91**, 220503(R) (2015).
[38] P.-Y. Liao, J.-K. Qin, G. Qiu, Y. Wang, W. Wu, and P. D. Ye, in *Xenes: 2D Synthetic Materials Beyond Graphene*, edited by A. Molle and C. Grazianetti (Woodhead Publishing, Kidlington, 2022), pp. 197–224, 10.1016/B978-0-12-823824-0.00004-6.
[39] G. Qiu, S. Huang, M. Segovia, P. K. Venuthurumilli, Y. Wang, W. Wu, X. Xu, and P. D. Ye, Nano Lett. **19**, 1955 (2019).
[40] S. Lin, W. Li, Z. Chen, J. Shen, B. Ge, and Y. Pei, Nat. Commun. **7**, 10287 (2016).
[41] H. Peng, N. Kioussis, and G. J. Snyder, Phys. Rev. B **89**, 195206 (2014).
[42] J. Qiao, Y. Pan, F. Yang, C. Wang, Y. Chai, and W. Ji, Sci. Bull. **63**, 159 (2018).
[43] Y. Wang, G. Qiu, R. Wang, S. Huang, Q. Wang, Y. Liu, Y. Du, W. A. Goddard, M. J. Kim, X. Xu *et al.*, Nat. Electron. **1**, 228 (2018).
[44] G. Zhou, R. Addou, Q. Wang, S. Honari, C. R. Cormier, L. Cheng, R. Yue, C. M. Smyth, A. Laturia, J. Kim *et al.*, Adv. Mater. **30**, 1803109 (2018).

[45] Q. Wang, M. Safdar, K. Xu, M. Mirza, Z. Wang, and J. He, ACS Nano **8**, 7497 (2014).
[46] L. Tong, X. Huang, P. Wang, L. Ye, M. Peng, L. An, Q. Sun, Y. Zhang, G. Yang, Z. Li *et al.*, Nat. Commun. **11**, 2308 (2020).
[47] J. Peng, Y. Pan, Z. Yu, J. Wu, J. Wu, Y. Zhou, Y. Guo, X. Wu, C. Wu, and Y. Xie, Angew. Chem. Int. Ed. **57**, 13533 (2018).
[48] K. Nakayama, A. Tokuyama, K. Yamauchi, A. Moriya, T. Kato, K. Sugawara, S. Souma, M. Kitamura, K. Horiba, H. Kumigashira *et al.*, Nature (London) **631**, 54 (2024).
[49] G. Qiu, C. Niu, Y. Wang, M. Si, Z. Zhang, W. Wu, and P. D. Ye, Nat. Nanotechnol. **15**, 585 (2020).
[50] N. Zhang, G. Zhao, L. Li, P. Wang, L. Xie, B. Cheng, H. Li, Z. Lin, C. Xi, J. Ke *et al.*, Proc. Natl. Acad. Sci. U. S. A. **117**, 11337 (2020).
[51] G. Gatti, D. Gosálbez-Martínez, S. S. Tsirkin, M. Fanciulli, M. Puppin, S. Polishchuk, S. Moser, L. Testa, E. Martino, S. Roth *et al.*, Phys. Rev. Lett. **125**, 216402 (2020).
[52] M. Sakano, M. Hirayama, T. Takahashi, S. Akebi, M. Nakayama, K. Kuroda, K. Taguchi, T. Yoshikawa, K. Miyamoto, T. Okuda *et al.*, Phys. Rev. Lett. **124**, 136404 (2020).
[53] T. Furukawa, Y. Shimokawa, K. Kobayashi, and T. Itou, Nat. Commun. **8**, 954 (2017).
[54] T. Yoda, T. Yokoyama, and S. Murakami, Sci. Rep. **5**, 12024 (2015).
[55] X. Huang, B. Liu, J. Guan, G. Miao, Z. Lin, Q. An, X. Zhu, W. Wang, and J. Guo, Adv. Mater. **30**, 1802065 (2018).
[56] C. Zhao, C. Tan, D.-H. Lien, X. Song, M. Amani, M. Hettick, H. Y. Y. Nyein, Z. Yuan, L. Li, M. C. Scott *et al.*, Nat. Nanotechnol. **15**, 53 (2020).
[57] X. Huang, R. Xiong, C. Hao, W. Li, B. Sa, J. Wiebe, and R. Wiesendanger, Adv. Mater. **36**, 2309023 (2024).
[58] Z. Zhu, X. Cai, S. Yi, J. Chen, Y. Dai, C. Niu, Z. Guo, M. Xie, F. Liu, J.-H. Cho *et al.*, Phys. Rev. Lett. **119**, 106101 (2017).
[59] X. Huang, J. Guan, Z. Lin, B. Liu, S. Xing, W. Wang, and J. Guo, Nano Lett. **17**, 4619 (2017).
[60] Y. Sun, T. Gotoh, B. Li, H. Li, and M. Zhu, Phys Status Solidi-R **18**, 2300414 (2024).
[61] G. Miao, J. Qiao, X. Huang, B. Liu, W. Zhong, W. Wang, W. Ji, and J. Guo, Phys. Rev. B **103**, 235421 (2021).
[62] See Supplemental Material at http://link.aps.org/supplemental/10.1103/PhysRevLett.133.236201 for materials and methods including sample fabrications, sample characterizations and DFT calculations, and additional experimental and calculational results, which includes Refs. [63–68].
[63] G. Kresse and J. Furthmüller, Phys. Rev. B **54**, 11169 (1996).
[64] P. E. Blöchl, Phys. Rev. B **50**, 17953 (1994).
[65] J. P. Perdew, J. A. Chevary, S. H. Vosko, K. A. Jackson, M. R. Pederson, D. J. Singh, and C. Fiolhais, Phys. Rev. B **46**, 6671 (1992).
[66] J. P. Perdew, K. Burke, and M. Ernzerhof, Phys. Rev. Lett. **77**, 3865 (1996).
[67] T. Filleter and R. Bennewitz, Phys. Rev. B **81**, 155412 (2010).
[68] K. E. Murphy, M. B. Altman, and B. Wunderlich, J. Appl. Phys. **48**, 4122 (1977).
[69] M. M. Ugeda, A. J. Bradley, S.-F. Shi, F. H. da Jornada, Y. Zhang, D. Y. Qiu, W. Ruan, S.-K. Mo, Z. Hussain, Z.-X. Shen *et al.*, Nat. Mater. **13**, 1091 (2014).
[70] P. Ebert, X. Chen, M. Heinrich, M. Simon, K. Urban, and M. G. Lagally, Phys. Rev. Lett. **76**, 2089 (1996).
[71] K.-J. Chao, C.-K. Shih, D. W. Gotthold, and B. G. Streetman, Phys. Rev. Lett. **79**, 4822 (1997).
[72] H. P. Ebert, Mater. Today **6**, 36 (2003).
[73] P. Ebert, T. Zhang, F. Kluge, M. Simon, Z. Zhang, and K. Urban, Phys. Rev. Lett. **83**, 757 (1999).
[74] S. Barja, S. Refaely-Abramson, B. Schuler, D. Y. Qiu, A. Pulkin, S. Wickenburg, H. Ryu, M. M. Ugeda, C. Kastl, C. Chen *et al.*, Nat. Commun. **10**, 3382 (2019).
[75] J. Drowart and P. Goldfinger, Q. Rev. Chem. Soc. **20**, 545 (1966).
[76] Data is available from Atomly: https://atomly.net/#/.